Food Hydrocolloids 121 (2021) 106977

Contents lists available at ScienceDirect

Food Hydrocolloids

journal homepage: www.elsevier.com/locate/foodhyd

# Impact of trehalose on physicochemical stability of β-carotene high loaded microcapsules fabricated by wet-milling coupled with spray drying

Liang Zhang, Yang Wei, Wenyan Liao, Zhen Tong, Yuan Wang, Jinfang Liu, Yanxiang Gao *

*Key Laboratory of Healthy Beverages, China National Light Industry Council, College of Food Science & Nutritional Engineering, China Agricultural University, Beijing, 100083, PR China*

ARTICLE INFO

*Keywords:*
β-Carotene
Trehalose
Microcapsule
Wet-milling
Physicochemical stability

ABSTRACT

Solvent-free β-carotene high loaded microcapsules formulated by octenyl succinic anhydride (OSA)-starch and trehalose were prepared by a combination of wet-milling and spray drying. The influence of different mass ratios of OSA-starch to trehalose on the particle size distribution, storage stability, hygroscopicity and redispersibility of β-carotene microcapsules was investigated. The optimized microcapsules exhibited a small average diameter (228.2 nm) after rehydration with high encapsulation efficiency and loading capacity (99.06% and 10.32%, respectively). The phase separation in the OSA-starch and trehalose composite matrix was observed in the presence of trehalose at a high level, which was favorable for the prominent storage stability of β-carotene (96.16% for 50 days). The half-life of rehydrated β-carotene microcapsules was also extended by 2.23- and 1.25-folds during the thermal- and photo-degradation treatments. The crystallinity of β-carotene microcapsules was largely reduced due to the enhanced hydrogen bonding interaction between OSA-starch and β-carotene as analyzed by FTIR. SEM images showed that the morphology of β-carotene microcapsules was regulated by the level of trehalose. Confocal Raman spectrum microscopy and hygroscopic variation jointly verified the entrapment of β-carotene into a glassy matrix formed at a high level of trehalose. Moreover, a high level of trehalose could improve the spontaneous sinkability and dispersibility of β-carotene microcapsules, which were completely rehydrated in less than 1 min.

## 1. Introduction

Poor solubility and stability are two major obstacles that restrict the application of hydrophobic bioactive ingredients in functional foods. Several well-known hydrophobic compounds such as β-carotene, curcumin, coenzyme Q10, astaxanthin and resveratrol belong to this type of food ingredients. Numerous scientists have attempted to overcome these drawbacks by various technological strategies, which can be roughly divided into the bottom-up and top-down approaches (Li et al., 2015). The bottom-up methods based on the spontaneous association of molecules, including anti-solvent precipitation (Wei, Yu, et al., 2019), emulsification evaporation (Wei et al., 2018) and chemical crosslinking (Kong et al., 2020), have suffered from various limitations in industrial production such as low loading capacity, residual organic solvents and thermodynamically unstable system (Colombo et al., 2018; Li et al., 2015). In comparison to the bottom-up processes, the top-down methods are mainly based on the mechanical size reduction through focused collision, shearing and friction stresses, which can offer the significant advantage of minimal use of chemical additives (Zhang et al., 2019). Most recently, the top-down methods have been widely reported to fabricate nanosuspensions, polymer nanoparticles and Pickering emulsions to improve the bioavailability and stability of poorly water-soluble ingredients (Colombo et al., 2018; Liu, Q. et al., 2020; Lu et al., 2018).

Wet-milling, an effective top-down method, is considered as the most promising and universal technique for the preparation of hydrophobic compound nano-delivery system, owing to its organic solvent-free treatment, high loading capacity (usually more than 5%) and easy scale-up of industrial production (Colombo et al., 2018; Semba et al., 2019). The milling-induced reduction in the average diameter of hydrophobic ingredients provides larger surface areas and thereby improves their physical stability and dissolution property. Up to date, many studies have concentrated on the preparation of bioactive compound nanosuspensions based on the wet-milling technique to enhance the saturation solubility and bioavailability. For example, Liu, Q. et al.

* Corresponding author. Box 112, No.17 Qinghua East Road, Haidian, District, Beiing, 100083, China.
*E-mail addresses:* zlcauer@126.com (L. Zhang), wy349@cau.edu.cn (Y. Wei), wenyanliaocau@126.com (W. Liao), tz527023029@163.com (Z. Tong), 18301576638@163.com (Y. Wang), jinfang.liu@cau.edu.cn (J. Liu), gyxcau@126.com (Y. Gao).

https://doi.org/10.1016/j.foodhyd.2021.106977
Received 27 February 2021; Received in revised form 20 May 2021; Accepted 17 June 2021
Available online 19 June 2021
0268-005X/© 2021 Elsevier Ltd. All rights reserved.

(2020) established the cilnidipine nanosuspension stabilized by a hydrophilic polymer and surfactant with excellent oral bioavailability and storage stability. The cilnidipine nanosuspension presented a narrow particle size distribution with an average size of 312 nm, and a remarkable increase of the dissolution rate in different media was observed compared with bulk cilnidipine. Nevertheless, liquid nanosuspensions are prone to be subjected to many inevitable instability problems, including precipitation, Ostwald ripening and crystal aggregation (Figueroa & Bose, 2013). Besides, nanosuspensions, because of their liquid media, are more likely to cause bacterial growth during transportation and storage (Malamatari et al., 2016). Therefore, the conversion of nanosuspensions to more convenient dosage forms (e.g. capsules, tablets, pellets etc.) is necessary to guarantee the adequate stability during storage.

Spray drying is such a common approach of solidification to manufacture microcapsule powders through the flash evaporation of liquid solvent by means of a hot drying gas. Compared with other drying methods, spray drying is quicker and more cost-effective to obtain powders with particular characteristics (e.g. morphology, moisture content and density) by adjusting the formulation and operating parameters (e.g. feed rate, inlet and outlet temperatures) (Malamatari et al., 2015). Despite of the fact that spray drying is feasible for the solidification of nanosuspensions, the exposure of nanosuspensions to intense desiccation stress may facilitate the transformation of crystal structure and alter the interfacial properties of nanosuspensions (Kumar et al., 2014). Especially in the high-loaded systems, water evaporates relatively quickly, and the adjacent nanoparticles tend to adhere to each other under the surface tension and van der Waals force, which may lead to the particle aggregation as well as the decrease of product solubility (Malamatari et al., 2016; Zuo et al., 2013). In order to solve these problems, several glycosyl carbohydrates, including sugars (e.g. maltose, lactose) and sugar alcohols (e.g. maltitol, xylitol), have been regarded as favorable matrix formers to prevent nanocrystal aggregation during spray drying and thereby improve the reconstitution performance of powders (Kumar et al., 2014).

As a potential matrix former for spray drying, trehalose is a natural non-reducing disaccharide consisting of two glucose molecules, which can interact intensively with the surface of macromolecules due to its great associativity and flexibility (Muhoza et al., 2020). Compared with other disaccharides, trehalose has a higher glass transition temperature (Tg, up to 120 °C) and is less hygroscopic, and these properties make trehalose an ideal flavor retention or protective agent for food-grade spray dried products. Moreover, trehalose is also effective on the preservation of vegetables and meats due to its crucial role in preventing starch retrogradation and protein degeneration (Cesàro et al., 2008; Wu et al., 2014). The impact of trehalose addition on physiochemical properties of various systems such as spray-dried carotenoid emulsion (Lim & Roos, 2017) and spray-dried lutein loaded layer-by-layer emulsion (Lim et al., 2016) have been investigated. The researchers found that trehalose played an important role in preventing the encapsulated components from agglomeration and degradation, and improving the redispersibility of powders. However, to the best of our knowledge, the physiochemical characteristics of β-carotene high loaded microcapsules fabricated by wet-milling coupled with spray drying, and the influence of trehalose concentration on the physicochemical properties of β-carotene high loaded nanosuspensions before or after spray drying have been not yet investigated.

In this work, the amphiphilic OSA-starch derived from esterification, which has been widely applied to encapsulate bioactive compounds for spray drying due to its superior emulsifying and film-forming properties, was applied as both the emulsifier and the wall material to formulate the β-carotene high loaded microcapsules. The monitoring mechanism of trehalose on enhancing the physicochemical stability of β-carotene microcapsules was elucidated in this study. To achieve this objective, the impact of OSA-starch and trehalose mass ratios on the particle size distribution, storage stability, hygroscopicity and spontaneous sinkability of β-carotene microcapsules was evaluated. Fourier transform infrared spectroscopy (FTIR) was employed to figure out the variation of intermolecular interactions between OSA-starch and β-carotene, and X-ray diffraction (XRD) was utilized to identify the crystalline transformation of β-carotene microcapsules on account of the incorporation of trehalose. Differential scanning calorimeter (DSC) was employed to detect heat flow related to phase transition of the microcapsules on the basis of temperature. The microstructure and relative phase distribution of spray-dried β-carotene microcapsules were characterized by scanning electron microscope (SEM) and confocal Raman spectrum microscopy (CRSM). The retention rate of β-carotene in the microcapsule powders was estimated at 55 °C during storge. The retention rate of β-carotene in the rehydrated microcapsules and milled nanosuspensions during thermal and light treatments was also evaluated to demonstrate the oxygen suppression of composite wall materials.

## 2. Materials and methods

### 2.1. Materials

β-Carotene (98% pure, UV method) was kindly provided by Xinhecheng Co., Ltd. (Xinchang, Zhejiang Province, China). Octenyl succinic anhydride (OSA)-modified waxy maize starch (HI-CAP 100, molecular weight: $9.6 \times 10^5$ g/mol, degree of substitution: 3.7%, moisture content: 6.32%, 32 < DE < 37) was purchased from Ingredion Company (Shanghai, China). Trehalose (>98%, crystalline dihydrate, molecular weight 342 Da) was purchased from Huiyang Biological Technology Co., Ltd. (Dezhou, Shandong Province, China). Hexane and ethanol with a purity of 99.99% were purchased from Beijing Chemical Works (Beijing, China).

### 2.2. Preparation of β-carotene high loaded microcapsules

β-Carotene high loaded microcapsules were fabricated by using the wet-milling and spray drying coupling technique. Firstly, OSA-starch was dissolved in 400 mL distilled water at 85 °C in water bath with magnetic stirring at 600 rpm until completely dissolved. Then, different weights (10, 30, 50, 60 and 70 g) of trehalose were added into OSA-starch solution to obtain five different OSA-starch to trehalose mass ratios of 9:1, 7:3, 5:5, 4:6 and 3:7. The sample without trehalose was set as the control group. Since β-carotene was hard to be well embedded when the trehalose level was higher than 70% (w/w) in the composite wall material, the OSA-starch to trehalose mass ratio of 3:7 was the limited level. After the solution was cooled to room temperature (25 °C), β-carotene crystal (15.0 g) was added to the OSA-starch and trehalose mixed solution and simultaneously homogenized at 8000 rpm by an Ultra-Turrax homogenizer (T25, Ika-Werke, Staufen, Germany) until the β-carotene crystal was completely dispersed. Subsequently, the resulting coarse suspension was added into a 1 L ball mill (FSW-1.0, Elemix, Shanghai, China) containing 2.5 kg zirconia beads (0.4–0.6 mm in diameter) with a circulating water cooler (the temperature was set to 5 °C). The milling process was performed by rotating the grind shaft at 2100 rpm for 150 min with the suspension temperature constant at around 20 °C. After milling, the obtained suspension was spray-dried (SD-BASIC, Labplant, UK) with the feed speed of 300 mL/h, input temperature of 165 °C and outlet temperature of 80 °C. The microcapsule powders were collected and stored in the refrigerator at −18 °C for further analysis.

### 2.3. Particle size and its distribution

The determination of particle size and polydispersity index (PDI) of rehydrated microcapsules and freshly milled nanosuspensions was analyzed with a Zetasizer Nano-ZS90 (Malvern Instruments, Worcestershire, UK) based on the principle of dynamic light scattering according to Wei, Zhang, et al. (2019). The particle size was obtained on

the basis of the Stokes-Einstein equation and expressed as cumulative average diameter. The rehydrated microcapsules (0.1%, w/v) were diluted 100 times with distilled water to avert multiple light scattering effect. All the measurements were conducted at room temperature in triplicate with each sample being balanced for 120 s.

### 2.4. Encapsulation efficiency and loading capacity of powdered microcapsules

The encapsulation efficiency and loading capacity of β-carotene high loaded microcapsules were determined according to Wei, Zhang, et al. (2019) with some modifications. The β-carotene was extracted from the rehydrated dispersion by using a mixture of absolute ethanol and n-hexane (1:3, v/v). The absorbance of the extract was analyzed with a UV-1800 spectrophotometer (Shimadzu Corporation, Kyoto, Japan) at a wavelength of 450 nm. The content of β-carotene was quantified by a standard curve of β-carotene ($y = 0.2623x + 0.0247$, $R^2 = 0.9996$). The encapsulation efficiency and loading capacity of β-carotene in the microcapsules were calculated by following the equations below:

$$Encapsulation\ efficiency\ (\%) = \frac{Encapsulated\ \beta - carotene}{Total\ \beta - carotene} \times 100\%$$

$$Loading\ capacity\ (\%) = \frac{Encapsulated\ \beta - carotene}{Total\ mass\ of\ microcapsule} \times 100\%$$

### 2.5. Differential scanning calorimeter (DSC)

The thermal behaviors of individual ingredients, β-carotene microcapsules and unloaded microcapsules were evaluated by a differential scanning calorimeter (TA Instruments, Newcastle, DE, United States). The melting peak temperature and enthalpy of β-carotene in the microcapsules were determined according to the method of Bilgili et al. (2018). Briefly, about 5 mg microcapsule powder was placed onto a standard aluminum pan and sealed tightly by a perforated aluminum slice. The obtained sample was heated from 25 to 185 °C at a constant rate of 10 °C/min with a constant purging of high purity nitrogen at a rate of 20 mL/min. An empty aluminum pan was regarded as the baseline. The glass transition temperature of the unloaded microcapsules (i.e. the microcapsules prepared by the wet-milling and spray drying coupling approach in the absence of β-carotene) was obtained by a heat-cool-heat cycle (Chen et al., 2020). Briefly, about 5 mg microcapsule powder was placed onto a standard aluminum pan and sealed tightly by a perforated aluminum slice. The sample was firstly heated to 160 °C at a rate of 20 °C/min and held at this temperature for 5 min, and then cooled down to −10 °C at a rate of 20 °C/min. After being equilibrated for 5 min, the sample was reheated to 160 °C at a rate of 20 °C/min, and the glass transition behavior was determined based on the second heating ramp. DSC patterns were analyzed by using universal analysis software (TA Instruments, Newcastle, DE, United States). The midpoint of the glass transition region was processed and defined as the glass transition temperature.

### 2.6. X-ray diffraction (XRD)

The crystallinity of the powders was determined by an X-ray diffractometer (Brucker D8, Odelzhausen, Germany). The individual ingredients and β-carotene microcapsules were evenly ground, respectively and then spread on the sample pool. The scan was ranged from 3° to 60° (2θ) with a step size of 0.02° and a step time of 5 s. X-ray diffraction patterns were analyzed by using software (MDI Jade 6) and calculated as relative crystallinity (%) according to the equation below (Lu et al., 2017):

$$Relative\ crystallinity\ (\%) = \frac{Sum\ of\ crystalline\ peak\ areas}{Total\ crystalline\ and\ amorphous\ peak\ areas} \times 100\%$$

### 2.7. Fourier transform infrared spectroscopy (FTIR)

The possible interactions among OSA-starch, trehalose and β-carotene were detected by a Spectrum 100 Fourier transform infrared spectrometer (PerkinElmer, Waltham, USA). Briefly, 2.0 mg microcapsule powder was mixed with 198 mg of desiccated potassium bromide and thoroughly ground, and pressed into flakes and tested under 64 scans at a wavenumber range from 4000 to 400 $cm^{-1}$ with a 4 $cm^{-1}$ resolution. The native potassium bromide flake was set as a baseline.

### 2.8. Observation of the microcapsule microstructure

#### 2.8.1. Optical microscopy

The microstructures of the rehydrated microcapsules and nanosuspensions were observed at 25 °C with an optical microscope (Leica 108, Heidelberg, Germany). The rehydrated solutions or nanosuspensions were pumped by an eyedropper and dropped onto the surface of the slide, then covered with a cover glass for observation.

#### 2.8.2. Confocal Raman spectrum microscopy

The phase composition and distribution of two components, namely OSA-starch and trehalose, in the unloaded microcapsules were detected by a confocal Raman microscopy (XperRam 200, Nanobase, Korea) since the presence of β-carotene could interfere with the detection of Raman signals (Chen et al., 2019). The excitation laser, laser power, exposure time and accumulation time were 532 nm, 15 mW, 5 s and 20 s, respectively. The Raman spectrum was obtained with a 1200 lines/mm grate ranging from 200 to 2760 $cm^{-1}$. A sweep range of 1600–1900 $cm^{-1}$, corresponding to the characteristic peak of carbonyl groups of OSA-starch, was analyzed to illustrate the phase distribution of OSA-starch in the microcapsules. Raman images were generated by using LabSpec 6 software. The red and green regions in the images denoted a high and low concentration of carbonyl groups, respectively.

#### 2.8.3. Scanning electron microscopy (SEM)

The microstructure of β-carotene high loaded microcapsules was acquired using a field emission scanning electron microscopy (SU8010, Hitachi, Tokyo, Japan). The microcapsule powders were placed onto a double faced adhesive tape covered by a thin layer of gold and observed under 10.0 kV acceleration voltage.

### 2.9. Bulk density, water activity and hygroscopic property of β-carotene microcapsules

The bulk density was determined by weighing 10 g of the microcapsule powder and then depositing into a 25 mL glass cylinder. The bulk density of the microcapsule powders was directly calculated by dividing the mass and volume; The water activity (Aw) was acquired by direct reading on a hygrometer (Aqualab, Pullman, United States) after the Aw value was stable; The hygroscopic property of β-carotene microcapsules and individual ingredients was investigated according to the method described by Cai and Corke (2000). Briefly, β-carotene microcapsule powders and individual ingredients were preliminarily dried by a moisture analyzer (MJ 33, Mettler Toledo, China) until the value was constant. Then, 0.2 g dried microcapsule powder was dispersed in culture dishes and placed into a desiccator with a preset saturated solution of $CaCl_2$, which corresponded to a relative humidity of 75% at 25 °C. The microcapsule powders were weighed once a day for a week and the hygroscopicity was expressed as the increase in mass per 100 g of powders by taking up water.

### 2.10. Spontaneous sinkability and dispersibility of β-carotene microcapsules

The spontaneous sinkability and dispersity of β-carotene microcapsule powders were assessed by a Turbiscan Lab Expert (Formulaction, France) on the basis of the backscattering and transmission detections of the microcapsules during sedimentation. Briefly, 1.5 g of powder sample was added into a borosilicate glass bottle containing 15 mL deionized water. Near-infrared light was utilized to scan glass bottles from bottom to top for 30 min with an interval of 25 s at 25 °C. The obtained spectrograms represented the change in the delta backscattering (ΔBS) and delta transmission (ΔT) of the sample as a function of the height of the glass bottle. The peak thickness and sediment velocity were calculated by Turbisoft 2.0 software with a selected area of the bottom of the bottle (ranging from 0 to 5 mm).

### 2.11. Stability of rehydrated β-carotene microcapsules and milled β-carotene nanosuspensions

#### 2.11.1. Physical stability

The physical stability of the rehydrated microcapsules and milled nanosuspensions was determined using a LUMi-Sizer (L.U.M. 290 GmbH, Germany) to expedite the appearance of flocculation and creaming (Wei et al., 2020). The samples were exposed to near-infrared light under the action of centrifugal pull to evaluate the transmission intensity. The measurement was operated with the liquid volume of 1.2 mL, rotational speed of 4000 rpm, operation time of 3600 s and time interval of 10 s.

#### 2.11.2. Thermal degradation kinetics

A first-order model was used to evaluate the thermal degradation kinetics of the β-carotene according to a method reported by Spada et al. (2012). Briefly, 1% (w/w) rehydrated microcapsules and nanosuspensions were placed in small transparent glass bottles and incubated at 80 °C for 1, 2, 3, 4 and 5 h in a thermostatic water bath and then cooled to 25 °C for β-carotene content analysis. The first-order degradation kinetic constant k and the half-life $t_{1/2}$ were calculated by following the equations below:

$$\ln(\frac{C}{C_0}) = -kt$$

$$t_{1/2} = \frac{\ln 2}{k}$$

In the equations above, $C_0$ and C represent the initial content and the content of β-carotene at the specified time, respectively.

#### 2.11.3. Light degradation kinetics

The first-order model aforementioned was also used to evaluate light degradation kinetics of β-carotene in the rehydrated microcapsules and milled nanosuspensions. Briefly, 1% (w/w) rehydrated microcapsules and nanosuspensions were placed into transparent light-specific bottles and incubated at a simulated light cabinet (light intensity: 0.35 w/$m^2$, temperature: 40 °C) (Q-Sun, Q-Lab Corporation, Ohio, USA), and the content of β-carotene in the samples was determined every 2 h for 10 h. The first-order degradation kinetic constant k and the half-life $t_{1/2}$ were calculated by following aforementioned equations in *2.11.2*.

#### 2.11.4. Storage stability

β-Carotene high loaded microcapsule powders were stored in a thermostatic storage bin (55 °C) for 50 days. The change of β-carotene retention in the absence or presence of air was simultaneously measured by using the method described earlier during storage.

### 2.12. Statistical analysis

All experiments were performed in triplicate. Mean ± standard deviation (SD) was utilized to express the experimental data, which was analyzed using the SPSS 20.0 software. Statistically significant differences were determined using one-way ANOVA followed by Turkey's multiple-comparison test. Difference was considered to be statistically significant as $p < 0.05$.

## 3. Results and discussion

### 3.1. Effect of wet-milling time on the characteristics of β-carotene suspensions and microcapsules

In order to better elucidate the transformation of β-carotene crystalline structure and the potential interaction between OSA-starch and β-carotene during wet-milling, the effect of wet-milling time on the characteristics of β-carotene suspensions and microcapsules stabilized by solely OSA-starch was preliminarily investigated. As shown in Fig. S1, with the extension of milling time, both the average diameter and polydispersity index (PDI) of β-carotene suspensions were decreased gradually, which could be explained by the pulverization of β-carotene crystals under the friction, collision, and shearing forces. Moreover, an equilibrium stage was achieved after milling for 150 min regardless of prolonging milling time, indicating that the diameter of β-carotene fine crystals was hard to be further minished due to the increased specific surface area and surface energy (Li et al., 2015; Monteiro et al., 2013). Similarly, both the encapsulation efficiency and loading capacity of β-carotene in the microcapsules were gradually increased with the extension of milling time (Fig. S2), suggesting that the amphiphilic OSA-starch was absorbed onto the surface of hydrophobic β-carotene crystals through the interaction between them (Bockuviene & Sereikaite, 2019). To verify this interaction, FTIR analysis was conducted and the result was shown in Fig. S3A. The spectrum of the physical mixture only exhibited the dominant absorption bands of β-carotene and OSA-starch, which confirmed that no obvious interaction occurred between the two components without milling. With extending milling time, the broad band corresponding to the O–H was eventually shifted from 3381.7 to 3372.8 $cm^{-1}$, unraveling that there existed hydrogen bonding interaction between amphiphilic OSA-starch and hydrophobic β-carotene. As for XRD analysis, the peak positions remained the same despite a slight reduction in the peak intensity for physical mixture (Fig. S3B), indicating the physical coverage of β-carotene crystals by OSA-starch. The relative crystallinity of the microcapsules was dramatically decreased to 20.83% after milling for 150 min, implying the partial amorphization of β-carotene and/or the formation of inclusion structure induced by wet-milling (Hecq et al., 2005).

### 3.2. Particle size and its distribution

The particle size and the size distribution of the milled nanosuspensions and rehydrated dispersions were presented in Fig. 1. The addition of trehalose exhibited scarcely impact on the particle size of the nanosuspensions, as the average diameter was all around 200 nm and had the similar narrow peaks of size distribution. Compared with the nanosuspensions, the size of the rehydrated dispersions was significantly ($p < 0.05$) increased and the size distribution became wider and more cluttered when the nanosuspensions were spray-dried into microcapsule powders and rehydrated. This result indicated that the agglomeration of β-carotene nanocrystals occurred during spray drying. As could be clearly found in the optical images, numerous carmine crystal aggregates were generated after drying and rehydration. This phenomenon was attributed to the dramatic decrease of both nucleation rate and supersaturation degree of β-carotene nanosuspensions during the rapid moisture evaporation (Malamatari et al., 2015). In addition, the high thermal stress-induced entanglement of starch chains and the

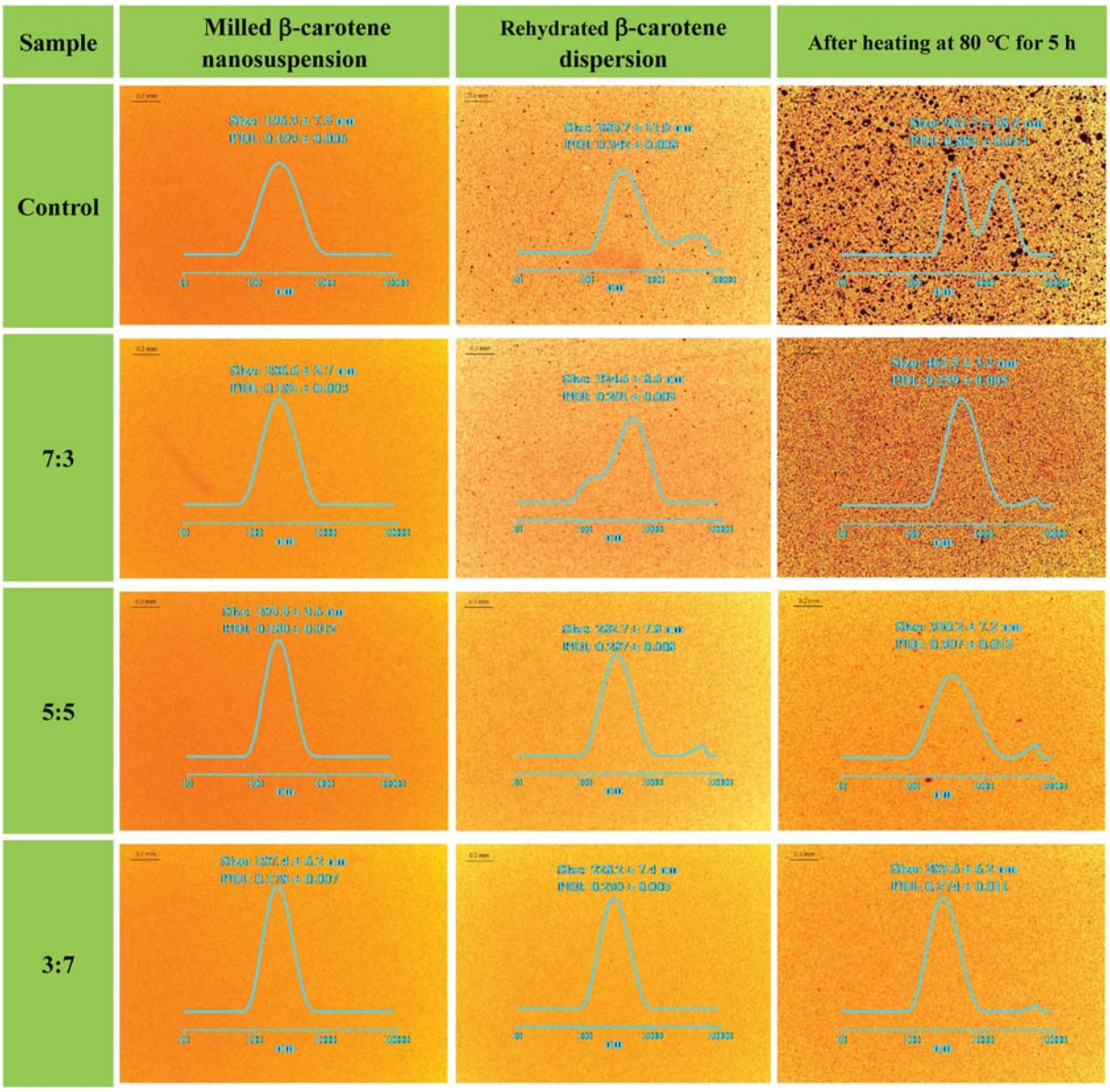


**Fig. 1.** Optical microscope images and particle size distribution of milled β-carotene nanosuspensions and rehydrated β-carotene dispersions (before and after heat treatment) with different OSA-starch to trehalose mass ratios.

inactivation of steric stabilization might further exacerbate this aggregation (Malamatari et al., 2015). However, with increasing the level of trehalose, there was a decreasing trend of the average diameter for the rehydrated dispersions. This result suggested that a higher level of trehalose could effectively prevent the high temperature-induced agglutination of β-carotene nanocrystals during spray drying, probably due to the reduced magnitude of interactions between starch molecules by intermolecular filling of trehalose, thus inhibiting the formation of crystal aggregates (Kumar et al., 2014; Yamasaki et al., 2011).

### 3.3. Encapsulation efficiency and loading capacity of β-carotene

The encapsulation efficiency was determined to guarantee the majority of β-carotene was well embedded inside the composite wall materials, otherwise the bioactive compound on the surface of microcapsules could directly contact with external environments (heat, $O_2$ and light), and thus resulted in degradation and isomerization of β-carotene (Zhan et al., 2020). The encapsulation efficiency and loading capacity of β-carotene high loaded microcapsules were shown in Fig. 2.

The encapsulation efficiency was gradually increased from 98.22% to 99.13% when the mass ratio of OSA-starch to trehalose was changed from 10:0 to 5:5, which was ascribed to the lower diffusion of β-carotene onto the microcapsule surface as a result of the improvement of microcapsule integrity (Kumar et al., 2014). Besides, the stronger spatial stability obtained in the presence of trehalose at a high level was also responsible for the superior integrity of the microcapsule structure (Muhoza et al., 2020). When the OSA-starch and trehalose mass ratio was lower than 5:5, the encapsulation efficiency reached the plateau, indicating that both the encapsulation and emulsifying capacity of OSA-starch were close to the limit as its concentration was less than 50% (w/w) in the composite wall material. The loading capacity of β-carotene was significantly ($p < 0.05$) decreased from 11.6% to 10.3% with the elevation of trehalose concentration. This result was presumably ascribed to that the binding sites of hydrophobic groups in the wall material became saturated when the mass ratio of OSA-starch and trehalose was 3:7, thus any additional β-carotene crystals could not be incorporated into the wall material (Guo et al., 2021). Absolutely, it could be supposed that OSA-starch, an amphiphilic macromolecular

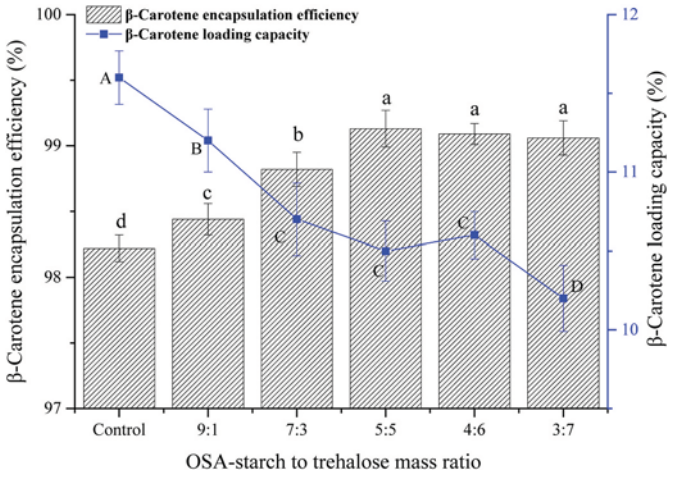


**Fig. 2.** Encapsulation efficiency and loading capacity of β-carotene in the microcapsules with different OSA-starch to trehalose mass ratios (Different superscript letters (a, b, c … A, B, C …) in the figure indicate significant differences ($p < 0.05$)).

wall material, played the essential role of encapsulation and emulsification in the preparation of β-carotene microcapsules, while trehalose lacked similar characteristics due to its low emulsifying property and the inability to balance the interfacial tension of the nanosuspensions (Han et al., 2020). Therefore, the OSA-starch and trehalose mass ratio of 3:7 was the limited level in this work.

### 3.4. FTIR and XRD

The infrared spectra of individual ingredients and β-carotene microcapsules with different OSA-starch to trehalose mass ratios were depicted in Fig. 3A. The strong bands located at 3027.2 and 2915.4 $cm^{-1}$ were identified as the characteristic skeleton stretching of C═C and aliphatic –CH groups of β-carotene crystal. The small peaks at 1712.6, 1559.6 and 1443.6 $cm^{-1}$ were assigned to the aromatic ring stretching, C═C bending and methylene deformation of carotenoids, respectively (Alma & Jolanta, 2019). However, these peaks were rarely observed in the spectra of the microcapsules, which confirmed that β-carotene was successfully encapsulated by the OSA-starch and trehalose composite matrix. The broad band corresponding to –OH groups of the microcapsules for the control group was shifted from 3401.5 $cm^{-1}$ to 3389.4 $cm^{-1}$, suggesting that hydrogen bonding interactions between β-carotene and OSA-starch occurred in the absence of trehalose (Kumar et al., 2014). With the incorporation of trehalose, the vibration intensity of FTIR spectra of the microcapsules was obviously increased and the peak of –OH group was further shifted from 3389.4 $cm^{-1}$ to 3332.1 $cm^{-1}$. These results implied that the hydrogen bonding interaction was further enhanced due to more available –OH groups derived from trehalose molecules (Kumar et al., 2014; Muhoza et al., 2020). To verify this statement, the FTIR analysis of the unloaded microcapsules was also performed to clarify the possible interaction between OSA-starch and trehalose in the absence of β-carotene. As shown in Fig. 3B, there was no obvious spectrum shift in the –OH group region regardless of increasing the level of trehalose, manifesting less or no interaction between the two components. This result was consistent with the finding of Jain and Roy (2008) that trehalose preferentially bound to water molecules rather than directly interact with the biomolecules either in dried powders or solutions. Furthermore, only single broad peak was found at 1026.9 $cm^{-1}$ despite increasing the level of trehalose and no new peak was generated in the range of 1047 to 995 $cm^{-1}$. This phenomenon demonstrated that the amorphous state of OSA-starch was well maintained even after the incorporation of crystalline trehalose.

The solubility and stability of hydrophobic bioactive ingredients

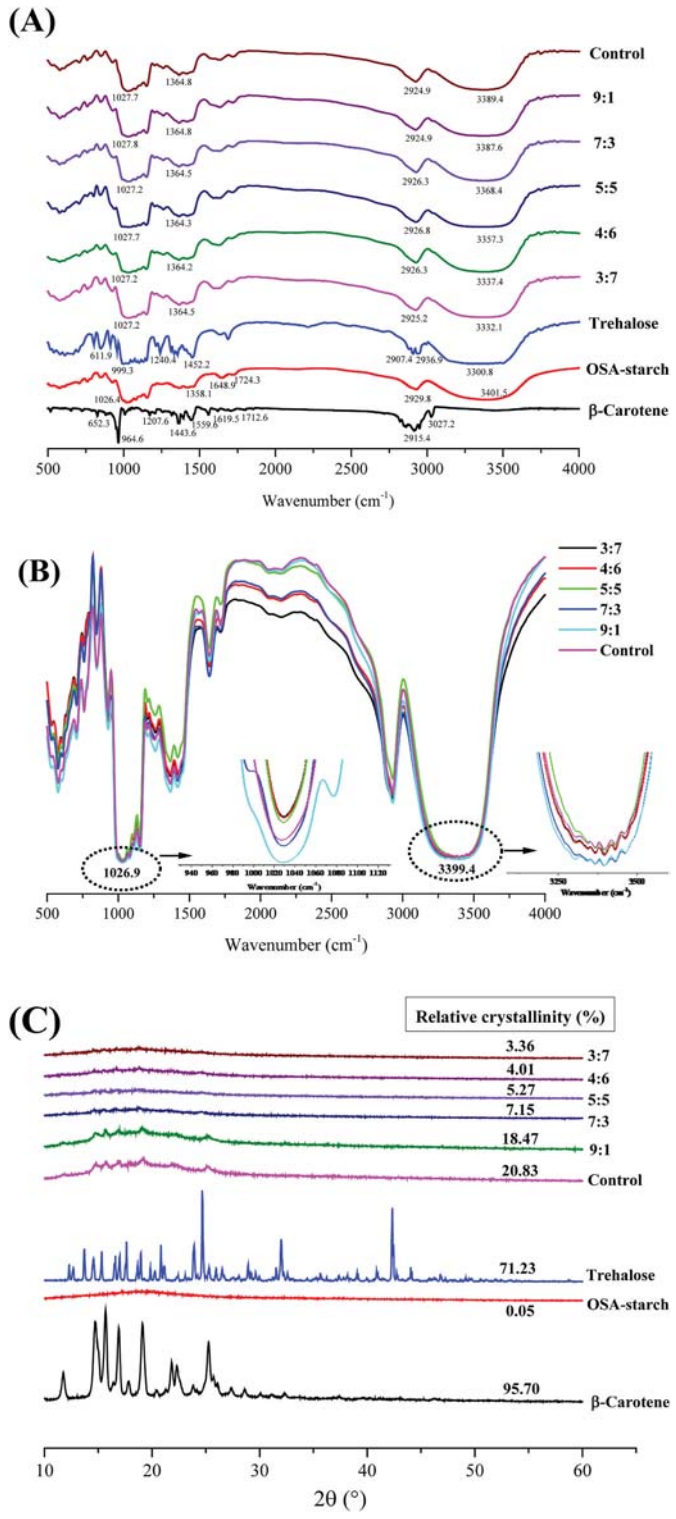


**Fig. 3.** FTIR analysis of individual ingredients, β-carotene loaded (A) and unloaded (B) microcapsules with different OSA-starch to trehalose mass ratios, and XRD (C) patterns of individual ingredients and β-carotene microcapsules with different OSA-starch to trehalose mass ratios.

were strongly associated with their crystalline states (Zhan et al., 2020). The crystalline diffraction patterns of individual ingredients and the microcapsules formulated by OSA-starch and trehalose at different mass ratios were presented in Fig. 3C. It could be observed that pure β-carotene and trehalose were highly crystallized with particularly sharp diffraction peaks occurring in the 2θ range of 10–25° and 15–45°,

respectively. Conversely, there was only one broad peak (19.3 ± 0.1°) in the diffraction pattern for OSA-starch, indicating the amorphous nature of the wall material. The peak intensity of the microcapsules decreased dramatically after milling process, which was attributed to the milling-induced transformation of crystalline structure of β-carotene (Alma & Jolanta, 2019). The absence of sharp diffraction peaks in trehalose suggested its existence as the amorphous nature after spray drying rather than crystalline state in the microcapsules, which was similar to the finding of Malamatari et al. (2015). When the level of trehalose increased, the relative crystallinity of the microcapsules was gradually decreased from 20.83% to 3.36% and reached its minimum at the OSA-starch and trehalose mass ratio of 3:7, which was consistent with the reduction of β-carotene crystalline aggregates and the average diameter of the rehydrated dispersions. The relatively low crystallinity of the final microcapsules could be ascribed to less breakage of the microcapsules and lower possibility of crystal agglomeration in the presence of trehalose at its high level (Kumar et al., 2014). The remaining crystallinity of 3.36% suggested that β-carotene was not completely transformed into the amorphous state after the wet-milling and spray drying coupling process, which was probably ascribed to that the presence of water triggered the recrystallization of partial amorphous β-carotene during wet-milling (Colombo et al., 2018; Malamatari et al., 2015).

### 3.5. DSC

As exhibited in Fig. S4, native β-carotene and trehalose were highly crystallized with strong endothermic peaks at specific temperatures, while OSA-starch scarcely presented any sharp melting peak due to its amorphous nature. The disappearance of endothermic peak for the incorporated trehalose indicated its existence as the amorphous distribution in the formation of microcapsules (Fig. 4A), which was confirmed by the XRD analysis aforementioned. The melting peak $T_m$ of β-carotene in the microcapsules was shifted to a lower temperature around 172 °C, indicating the reduction in crystallinity due to the decreased particle size of β-carotene as well as the favorable hydrogen bonding interaction between OSA-starch and β-carotene (Lv et al., 2019). With increasing the level of trehalose, the fusion enthalpy $\Delta H_m$ corresponding to the melting of β-carotene was gradually decreased, unraveling that less energy was required to melt β-carotene in the microcapsules with reduced cohesive energy (Bilgili et al., 2018). This result might be owing to that trehalose promoted the formation of β-carotene crystal defects and crystal lattice disorders during spray drying, which further confirmed the partial amorphization of crystalline β-carotene (Liu, Q. et al., 2020). The lowest $\Delta H_m$ of 10.2 J/g was obtained at the OSA-starch to trehalose mass ratio of 3:7, manifesting that less crystal aggregates were generated and the integrity of the microcapsules was well maintained in the presence of trehalose at its high level.

The vitrification of the unloaded microcapsules was also detected in order to explore the pivotal components that affected the microcapsule characteristics. According to the report of da Silva Carvalho et al. (2016), the glass transition temperature of the microcapsule powders was not only depended on the Tg of the wall material but also related to the interactions among individual ingredients. As shown in Fig. 4B, only single Tg was found when the mass ratio of OSA-starch to trehalose was higher than 7:3, indicating the good compatibility and miscibility of both components in the presence of trehalose at its low level. When the level of trehalose was further increased, two Tgs were observed, which verified the occurrence of amorphous-amorphous phase separation in the OSA-starch and trehalose composite matrix. Hughes et al. (2016) reported that phase separation promoted to form a denser molecular structure and reduced free volume of the carbohydrate polymer matrix, which was consistent with our findings in terms of micromorphology and storage stability of the microcapsules. Compared with the study of Chen et al. (2019), the Tg of OSA-starch and trehalose matrix was higher than that of OSA-starch and sucrose matrix in the case of phase

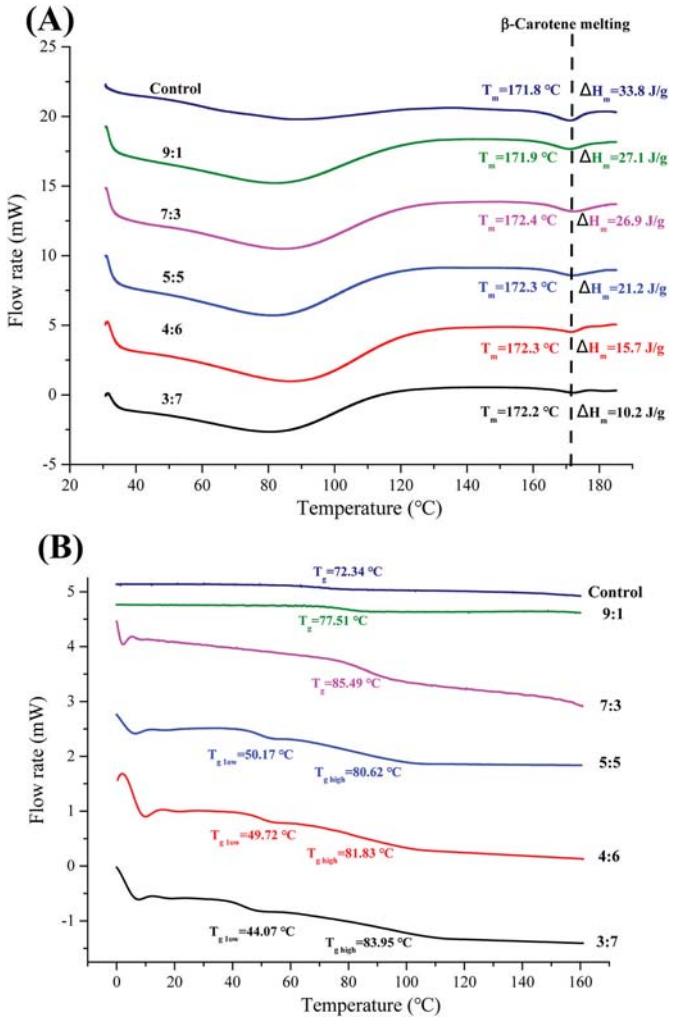


**Fig. 4.** DSC curves of β-carotene loaded (A) and unloaded (B) microcapsules with different OSA-starch to trehalose mass ratios.

separation. This phenomenon could be explained by the preferential exclusion theory that the addition of trehalose to bulk water sequestered water molecules away from the biopolymers, suppressing the reduction in Tg of the composite matrix in the absence of water as a plasticizer (Hughes et al., 2018; Jain & Roy, 2008).

### 3.6. SEM and CRSM

During spray drying, the rapid dehydration of wall materials occurs due to the flash evaporation of water, resulting in uneven shrinkage or structural fracture of the microcapsule surface. As shown in Fig. 5A, the microcapsules without trehalose exhibited obvious ruptures and wrinkles, revealing that the chain structure of starch molecules was not firm enough to encapsulate β-carotene at a high level in the absence of trehalose, which was in agreement with the relatively low encapsulation efficiency and poor redispersibility of the microcapsules. Interestingly, some of the microcapsules retained their completely spherical shape with the smooth surface, whereas their insides were hollow. This phenomenon could be explained by the "ballooning effect" that the microcapsules were blown up by the inlet hot air during spray drying due to the poor rigidity of wall materials and the incompact construction of the microcapsules. The formation of air vesicles, which could lead to the fracture of microcapsules, was reported at higher exhaust temperatures during spray drying (Salminen et al., 2019). With increasing the level of trehalose, the probability of the particle rupturing was decreased, and

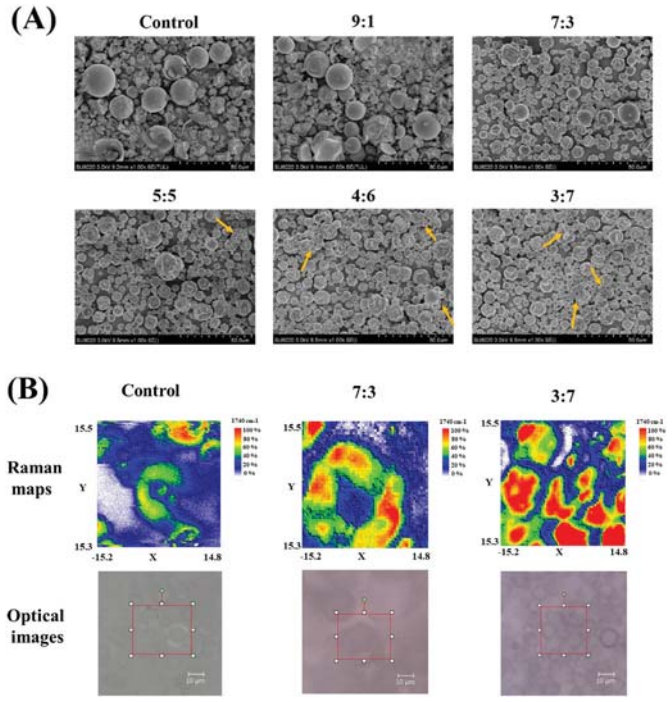


**Fig. 5.** SEM (A) images of powdered β-carotene microcapsules and CRSM (B) images of unloaded microcapsules with different OSA-starch to trehalose mass ratios.

the inflated microcapsules with the smooth surface and large particle size were barely detected. The result revealed that the incorporation of trehalose contributed to the reduction of free volume between β-carotene and wall materials since less air was encased inside the microcapsules, resulting in the decrease of the particle size. The diminishment of free volume was consistent with the increase of poured bulk density of the microcapsules shown in Table 1. When the concentration of trehalose was further elevated, slight aggregation of the microcapsules was observed, which could be attributed to bridging agglomeration by the excessive trehalose molecules (Muhoza et al., 2020).

Confocal Raman spectrum microscopy was employed to figure out the phase distribution of the wall materials based on the interactions between the excitation light and samples (Liu, X. et al., 2020). The direct visualization of phase distribution between OSA-starch and trehalose in the unloaded microcapsules was displayed in Fig. 5B. The optical maps exhibited opportunely the same regions mapped by the Raman microscope, while the Raman maps uncovered the molecular distribution. The red and green regions in the Raman maps represented a high and low concentration of carbonyl groups, respectively. In the control sample, the green regions were continuously distributed in the powder, indicating the relatively uniform dispersion of OSA-starch in the internal and external parts of the microcapsules (Liu et al., 2016). After the incorporation of trehalose, a blended region containing both high and low concentrations of carbonyl groups were detected around the outer part of the microcapsule. This result confirmed the favorable compatibility and miscibility of trehalose and OSA-starch in the microcapsules due to their hydrophilic nature (Liu, X. et al., 2020). When the level of trehalose was further elevated, the relative distribution of carbonyl groups in the microcapsules was altered greatly. The carbonyl groups were independently dispersed in the powder without any adhesions, and most of them were concentrated in the interior of the microcapsules to form red regions, manifesting the formation of a layer-by-layer structure in the microcapsules. This phenomenon could be explained by the phase separation that the blend of OSA-starch and trehalose no longer existed as a heterogeneous phase after spray drying in the presence of trehalose at a high level, and the starch phase tended to be assembled due to the differences in viscosity and molecular weight of the two components (Chen et al., 2019; Kilpeläinen et al., 2020). In this case, the outer trehalose around the inner starch could act as a dense barrier that effectively prevented oxygen from penetration, and this layer-by-layer structure could explain why β-carotene became much more stable in the presence of trehalose at a high level.

**Table 1**
The water activity and bulk density of OSA-starch, trehalose and β-carotene microcapsules with different mass ratios of OSA-starch to trehalose.

| Sample | Water activity | Bulk density (g/mL) |
|---|---|---|
| OSA-starch | $0.245 \pm 0.003^{e}$ | $0.49 \pm 0.01^{d}$ |
| Trehalose | $0.438 \pm 0.006^{a}$ | $0.85 \pm 0.01^{a}$ |
| Microcapsule $_{control}$ | $0.302 \pm 0.005^{b}$ | $0.52 \pm 0.02^{c}$ |
| Microcapsule $_{9:1}$ | $0.305 \pm 0.002^{b}$ | $0.53 \pm 0.02^{c}$ |
| Microcapsule $_{7:3}$ | $0.301 \pm 0.007^{b}$ | $0.57 \pm 0.01^{c}$ |
| Microcapsule $_{5:5}$ | $0.289 \pm 0.004^{c}$ | $0.63 \pm 0.02^{b}$ |
| Microcapsule $_{4:6}$ | $0.284 \pm 0.003^{c}$ | $0.66 \pm 0.01^{b}$ |
| Microcapsule $_{3:7}$ | $0.273 \pm 0.003^{d}$ | $0.68 \pm 0.01^{b}$ |

Values are means ± SD (n = 3). Different superscript letters (a, b, c, d and e) in the same column indicate significant differences ($p < 0.05$).

### 3.7. Water activity (Aw) and hygroscopic property

Water activity (Aw) is a common indicator to predict the storage stability of the microcapsule powders. Generally, several undesirable phenomena can take place such as caking, crystallization or stickiness in powders with high Aw and moisture hygroscopicity. Additionally, there exists a negative correlation between Aw and vitrification transition of food components, i.e. once the Aw decreases, the Tg increases. Among the samples in Table 1, trehalose exhibited the highest Aw of 0.438 ± 0.006 due to its dihydrate crystalline nature, while OSA-starch had a relatively low Aw of 0.245 ± 0.003. The results indicated that the Aw values of all the spray-dried microcapsules ranged from 0.273 ± 0.003 to 0.305 ± 0.002, unraveling that the side reactions including enzymatic reaction and microbial growth were well inhibited under such low Aw. The decreased Aw value of the microcapsules revealed that anhydrous trehalose was obtained due to the rapid evaporation of moisture during spray drying. The lowest Aw was found at the OSA-starch and trehalose mass ratio of 3:7, which was attributed to that the large quantity of trehalose preferentially bound to water molecules on the starch surface, leading to the formation of an effective moisture absorption layer, thus facilitating the water transmission from the external surface of the microcapsules during spray drying (Muhoza et al., 2020). Due to the lower Aw, the microcapsules at the OSA-starch and trehalose mass ratio of 3:7 might exhibit a superior retention rate of bioactive compounds during the storage.

Hygroscopicity was measured for the microcapsule powders to gain an insight into their physical stability in case of storage under a high humidity atmosphere. The moisture adsorption kinetics of the preliminarily dried microcapsules was shown in Fig. 6, by means of relative moisture increment as a function of time. Compared with the dried OSA-starch, the anhydrous trehalose exhibited a faster rate of moisture absorption and a relatively higher hygroscopicity of 5.45 ± 0.08 g/100 g after storage for one week. All the microcapsule powders showed high hygroscopicity with the final moisture adsorption ranging from 4.26 ± 0.15 to 5.19 ± 0.03 g/100 g. Faster moisture adsorption rate was found in the samples on the first 2 days and turned slower in the following days. Noteworthily, when the level of trehalose was relatively low, the hygroscopicity of the microcapsules was slightly restricted. This result could be explained by the water replacement theory that the water molecules absorbed onto the surface of the microcapsules could be substituted by the trehalose-forming hydrogen bonds, which could maintain the three-dimensional structure of the microcapsules and retard the intrusion and diffusion of moisture through the micropores of the microcapsules (Jain & Roy, 2008; Muhoza et al., 2020).

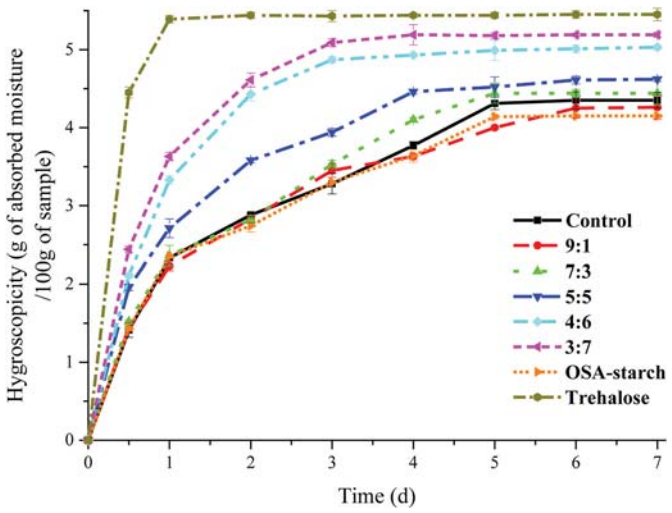


**Fig. 6.** Hygroscopic property of powdered β-carotene microcapsules with different OSA-starch to trehalose mass ratios.

Nevertheless, the hygroscopicity of the microcapsules was increased with elevating the trehalose level when the mass ratio was lower than 9:1. This gradual increment reflected that excessive trehalose located on the outer layer of the microcapsules promoted the vapor absorption. The anhydrous trehalose in the amorphous state exhibited an easier moisture adsorption due to the presence of more numbers of hydrophilic groups and short chains (da Silva Carvalho et al., 2016). Moreover, the water adsorption rate of the microcapsules constituted by trehalose at a high level was much faster than that at a low level, thus verifying that the outer layer of the microcapsules was filled with a large amount of trehalose. The variation in the hygroscopic property of the microcapsules further confirmed the entrapment of β-carotene into the glassy matrix formed at a high level of trehalose.

### 3.8. Spontaneous sinkability and dispersibility

Sinkability and dispersibility are two important factors to assess the quality of powdered microcapsules. As displayed in Fig. 7A, negative ΔBS values with uneven spectral curves were detected for the control group and the sample with a low level of trehalose, indicating their heterogeneous and relatively slow settlement. With increasing the level of trehalose, the final ΔBS of the microcapsules was elevated from 40% to 60%, and the spectral curves of ΔT were barely altered during measurement. This result manifested that more powders settled to the bottom of glass bottle at a faster sinking velocity, and a homogeneous rehydration system was consequently obtained, which was further confirmed by the optical scan images shown in Fig. S5. The variation of peak thickness located in the bottom of the glass bottle was shown in Fig. 7B. The peak thickness of the sample with a high level of trehalose was much larger than that of the control group, and the slope of peak thickness was increased from 4.95 mm/h to 105.99 mm/h. This result also confirmed the crucial role of trehalose in improving the redispersibility of the microcapsule powders. The enhanced instant solubility might be ascribed to the increasing the wettability of the powdered microcapsules (Kumar et al., 2014). Since the wettability of sugars was superior compared to that of polysaccharides, the wettability of the microcapsules consisting of a high level of trehalose was largely enhanced. In this case, the adsorption capacity of water on the surface of the microcapsules was stronger, and the outer layer of the microcapsules could be wetted more quickly (Yamasaki et al., 2011). In addition, a higher bulk density of the microcapsules was also favorable for the improved dispersibility of the microcapsules, because food powders with a larger bulk density could be rehydrated more easily than those with a smaller bulk density due to their better penetration performance (Camargo Novaes et al., 2019). Moreover, the existence of planetary agglomerations surrounded by many small microcapsule particles as observed in SEM images was also responsible for the enhanced dissolution. On one hand, these surrounded microcapsule particles had smaller sizes with greater specific surface areas, and thus exhibited a more prominent wettability; on the other hand, there existed the formation of capillary effect during rehydration (indicated by the yellow arrow in Fig. 7C) due to this unique aggregate structure, which could facilitate the moisture penetration through capillary interstice between the microcapsules and small particles (Wu et al., 2019).

### 3.9. Physicochemical stability

#### 3.9.1. Physical stability

The stability of the rehydrated dispersions was indicated as the evolution of the transmission-space profiles during centrifugation. The curve of instability index as a function of time presented an intuitive insight into the difference in physical stability of the nanosuspensions and their rehydrated dispersions (Fig. 8A), and the lower instability index corresponded to the better physical stability (Zhan et al., 2020).

The nanosuspensions were much more stable than their rehydrated dispersions because of the smaller average diameter (around 190 nm) of the nanosuspensions, and there seemed to be no difference in the stability of distinct nanosuspensions due to their similar particle size distribution and optical microstructure. With regard to the rehydrated dispersions, the higher level of trehalose was conducive to the improvement of stability, which could be deduced from the less variation of the integrated transmissions and the smaller instability indexes. This result might be ascribed to the dominant role of trehalose in maintaining the particle size of the microcapsules during spray drying. In the case of strong thermal stress from spray drying, the β-carotene microcapsules encapsulated by single OSA-starch tended to be damaged, and the interior β-carotene crystals were more likely to be aggregated, which increased the sedimentation velocity of the rehydrated microcapsules (Malamatari et al., 2015).

#### 3.9.2. Thermal stability and photostability

The degradation kinetics of the microcapsules during the exposure to UV light irradiation or thermal treatment was investigated. The slope value (k), half-life ($t_{1/2}$), and correlation coefficient ($R^2$) were calculated from the fitted linear equations and summarized in supplementary information tables (Tables S1 and S2).

The thermal degradation kinetics of the nanosuspensions and rehydrated microcapsules with different OSA-starch and trehalose mass ratios were shown in Table S1. It could be found that the $t_{1/2}$ values of the nanosuspensions were much higher than those of the rehydrated microcapsules. This result suggested that adverse effects associated with the physicochemical stability of the nanosuspensions occurred after spray drying. Furthermore, crystalline aggregates were hardly observed after heating with a high level of trehalose. The thermal stability of both β-carotene nanosuspensions and rehydrated microcapsules was also improved during heating as the level of trehalose increased. This result might be owing to that less oxygen could be dissolved into the liquid system in the presence of more number of hydroxyl groups (Chen et al., 2019). Penicaud et al. (2012) also declared that the oxygen solubility and diffusivity were restricted when sucrose concentration increased, and the oxygen solubility could be expressed as a function of sucrose concentration.

The light degradation kinetics of the nanosuspensions and rehydrated microcapsules with different OSA-starch and trehalose mass ratios were also conducted (Table S2). The $t_{1/2}$ values of β-carotene in different nanosuspensions were increased from 14.53 h (without trehalose) to 14.69, 16.42, 17.07, 17.32 and 17.55 h for the nanosuspensions with the OSA-starch and trehalose mass ratios of 9:1, 7:3, 5:5, 4:6, 3:7, respectively. Similarly, the $t_{1/2}$ values of β-carotene in distinct rehydrated microcapsules were also increased. These results

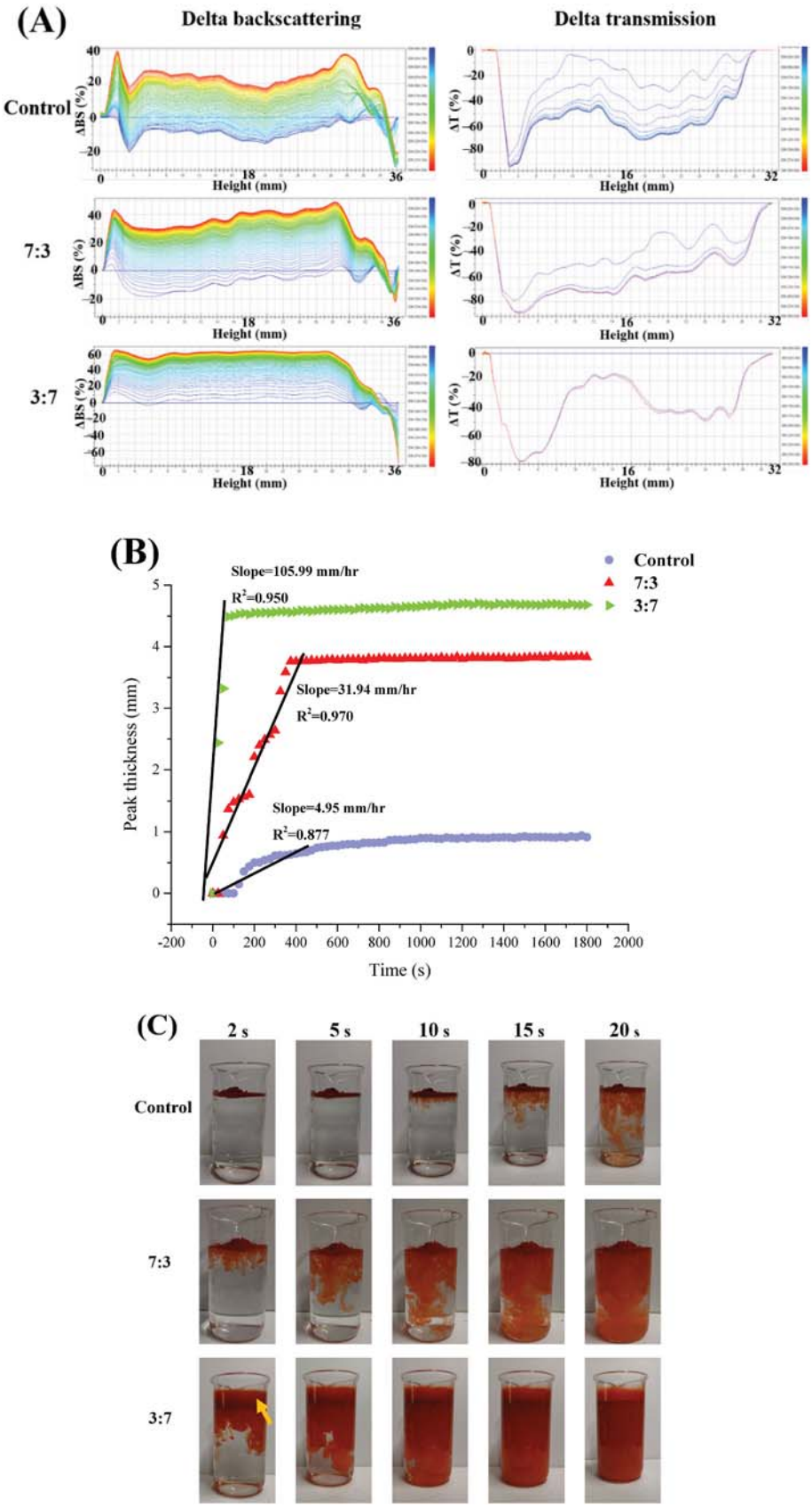


**Fig. 7.** Delta Backscattering and delta transmission (A), peak thickness (B) and spontaneous settlement (C) of β-carotene microcapsules with different OSA-starch to trehalose mass ratios.

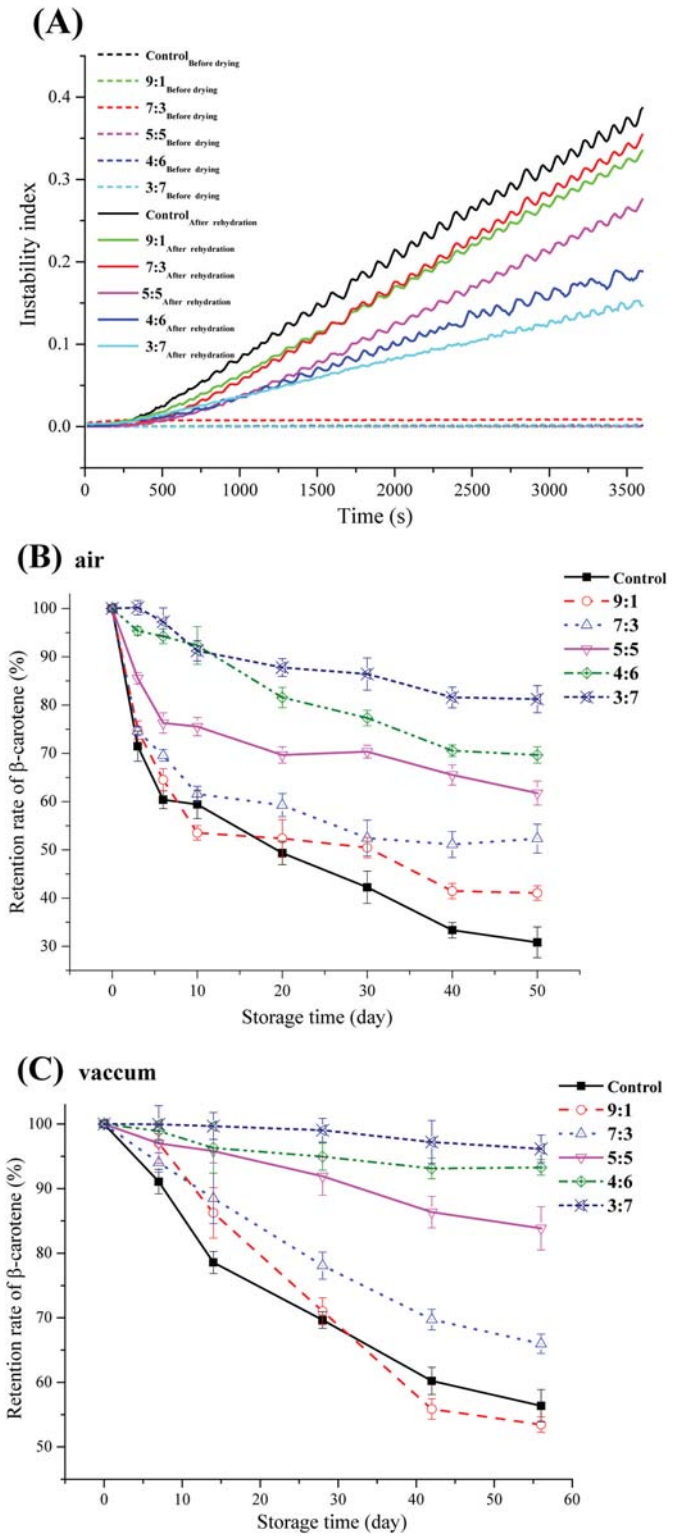


**Fig. 8.** Physical stability (A) and storage stability (B, C) of powdered β-carotene microcapsules in the presence or absence of oxygen.

revealed that β-carotene embedded in the composite wall material became more stable, and the increasing trehalose concentration was also favorable to the photostability of all the samples. This result could be ascribed to that the chemically reactive groups of β-carotene were effectively protected from UV irradiation through the formation of a denser protective carrier at a high level of trehalose.

### 3.9.3. Storage stability

Enhancing the air impermeability and oxygen resistance of wall materials is of great importance to the storage performance and commercial application of the microcapsules. The spray-dried microcapsule powders with different OSA-starch to trehalose mass ratios were stored in the presence or absence of air (Fig. 8B and C) at 55 °C to explore whether the microcapsules were still stable under a long-term storage. The difference of β-carotene retention rate became more obvious when stored in contact with air, indicating that the presence of oxygen accelerated the chemical degradation of β-carotene. The β-carotene in the microcapsules with a high level of trehalose presented a better retention rate around 95%, which was much higher than that with a low level of trehalose (around 55%). The improved storage stability of the microcapsules with a high level of trehalose could be explained by two aspects. On one hand, the incorporation of trehalose conduced to the reduction of free volume between β-carotene and the wall material, leaving less air encased inside the microcapsules; on the other hand, the compact glassy matrix formed at a high level of trehalose was considered as an effective oxygen barrier so that less oxygen could infiltrate into the microcapsules through fine holes on the wall material surface. Likewise, Boerekamp et al. (2019) also found that the reduction of free volume was responsible for the limited oxygen permeability and diffusivity of fish oil-loaded microcapsules. Apart from the two main reasons above, the microcapsules were stored at 55 °C, which was lower than the Tg of the wall materials, suggesting that the glassy state of the wall materials was maintained during storage. In this case, the wall materials behaved like solids and the mobility of starch chains in the glassy matrix was largely limited, which could effectively prevent oxygen from infiltration (Chen et al., 2019).

## 4. Conclusion

In this study, β-carotene high loaded microcapsules were successfully fabricated by wet-milling coupled with spray drying. Trehalose acted as a glassy matrix former or hydroxyl groups supplier in the formation of β-carotene microcapsules. As the level of trehalose was increased, the physicochemical stability of both β-carotene microcapsule powders and rehydrated dispersions was obviously improved. The incorporation of trehalose was favorable to preventing β-carotene nanocrystals from agglutination during spray drying due to the enhancement of hydrogen bonding interactions between β-carotene and OSA-starch. The phase separation of the wall material occurred in the presence of trehalose at a high level, which could effectively prevent oxygen from penetration. The reduced free volume of the β-carotene microcapsules was responsible for their prominent storage stability since less oxygen could be encased inside the microcapsules. The stability of both β-carotene nanosuspensions and rehydrated microcapsules was also increased due to the reduction in the solubility and diffusivity of oxygen in the presence of more hydroxyl groups. Furthermore, the microcapsules formulated with a high level of trehalose exhibited the instant dissolution property due to the enhanced wettability and the existence of planetary agglomerations.

## CRediT authorship contribution statement

**Liang Zhang:** Conceptualization, Methodology, Software, Writing – original draft, preparation, Data curation. **Yang Wei:** Formal analysis, Investigation. **Wenyan Liao:** Formal analysis, Investigation. **Zhen Tong:** Formal analysis, Investigation. **Yuan Wang:** Formal analysis, Investigation. **Jinfang Liu:** Writing – review & editing. **Yanxiang Gao:** Conceptualization, Supervision, Project administration, Funding acquisition, Writing – review & editing.

## Declaration of competing interest

The authors declare no competing financial interest.

## Acknowledgment

The research was funded by the National Natural Science Foundation of China (No. 31871842). We acknowledge Ying Ye from the Aunion Tech Co., Ltd, China, for performing the confocal Raman spectrum microscopy analysis.

## Appendix A. Supplementary data

Supplementary data to this article can be found online at https://doi.org/10.1016/j.foodhyd.2021.106977.

## References

Alma, B., & Jolanta, S. (2019). Preparation and characterisation of novel water-soluble β-carotene-chitooligosaccharides complexes. *Carbohydrate Polymers, 225*, 115226.
Bilgili, E., Rahman, M., Palacios, D., & Arevalo, F. (2018). Impact of polymers on the aggregation of wet-milled itraconazole particles and their dissolution from spray-dried nanocomposites. *Advanced Powder Technology, 29*, 2941–2956.
Bockuviene, A., & Sereikaite, J. (2019). Preparation and characterisation of novel water-soluble β-carotene-chitooligosaccharides complexes. *Carbohydrate Polymers, 225*, 115226.
Boerekamp, D. M. W., Andersen, M. L., Jacobsen, C., Chronakis, I. S., & Garcia Moreno, P. J. (2019). Oxygen permeability and oxidative stability of fish oil-loaded electrosprayed capsules measured by Electron Spin Resonance: Effect of dextran and glucose syrup as main encapsulating materials. *Food Chemistry, 287*, 287–294.
Cai, Y. Z., & Corke, H. (2000). Production and properties of spray-dried Amaranthus betacyanin pigments. *Journal of Food Science, 65*(7), 1248–1252.
Camargo Novaes, S. S., Hellmeister Dantas, F. B., Alvim, I. D., Rauen de Oliveira Miguel, A. M., Vissotto, F. Z., & Vercelino Alves, R. M. (2019). Experimental method to obtain a uniform food powder mixture of omega-3 microcapsules and whole milk powder. *Lebensmittel-Wissenschaft & Technologie, 102*, 372–378.
Cesàro, A., De Giacomo, O., & Sussich, F. (2008). Water interplay in trehalose polymorphism. *Food Chemistry, 106*(4), 1318–1328.
Chen, X., Liang, R., Zhong, F., Ma, J., John, N.-A., Goff, H. D., & Yokoyama, W. H. (2019). Effect of high concentrated sucrose on the stability of OSA-starch-based beta-carotene microcapsules. *Food Hydrocolloids, 12*, 105–118.
Chen, S., Li, Q., McClements, D. J., Han, Y. H., Dai, L., Mao, L. K., & Gao, Y. X. (2020). Co-delivery of curcumin and piperine in zein-carrageenan core-shell nanoparticles: Formation, structure, stability and in vitro gastrointestinal digestion. *Food Hydrocolloids, 99*.
Colombo, M., Minussi, C., Orthmann, S., Staufenbiel, S., & Bodmeier, R. (2018). Preparation of amorphous indomethacin nanoparticles by aqueous wet bead milling and in situ measurement of their increased saturation solubility. *European Journal of Pharmaceutics and Biopharmaceutics, 125*, 159–168.
Figueroa, C. E., & Bose, S. (2013). Spray granulation: Importance of process parameters on in vitro and in vivo behavior of dried nanosuspensions. *European Journal of Pharmaceutics, 85*(3), 1046–1055.
Guo, Q., Su, J., Shu, X., Yuan, F., Mao, L., Liu, J., & Gao, Y. (2021). Fabrication, structural characterization and functional attributes of polysaccharide-surfactant-protein ternary complexes for delivery of curcumin. *Food Chemistry, 337*, 128019.
Han, C., Xiao, Y., Liu, E., Su, Z., Meng, X., & Liu, B. (2020). Preparation of Ca-alginate-whey protein isolate microcapsules for protection and delivery of L. bulgaricus and L. paracasei. *International Journal of Biological Macromolecules, 163*, 1361–1368.
Hecq, J., Deleers, M., Fanara, D., Vranckx, H., & Amighi, K. (2005). Preparation and characterization of nanocrystals for solubility and dissolution rate enhancement of nifedipine. *International Journal of Pharmaceutics, 299*(1–2), 167–177.
Hughes, D. J., Bönisch, G. B., Zwick, T., Schäfer, C., Tedeschi, C., Leuenberger, B., Martini, F., Mencarini, G., Geppi, M., Alam, M. A., & Ubbink, J. (2018). Phase separation in amorphous hydrophobically modified starch–sucrose blends: Glass transition, matrix dynamics and phase behavior. *Carbohydrate Polymers, 199*, 1–10.
Hughes, D., Tedeschi, C., Leuenberger, B., Roussenova, M., Coveney, A., Richardson, R., Bönisch, G. B., Alam, M. A., & Ubbink, J. (2016). Amorphous-amorphous phase separation in hydrophobically-modified starch–sucrose blends II. Crystallinity and local free volume investigation using wide-angle X-ray scattering and positron annihilation lifetime spectroscopy. *Food Hydrocolloids, 58*, 316–323.
Jain, N. K., & Roy, I. (2008). Effect of trehalose on protein structure. *Protein Science : A Publication of the Protein Society, 18*, 24–36.
Kilpeläinen, T., Pajula, K., Ervasti, T., Uurasjärvi, E., Koistinen, A., & Korhonen, O. (2020). Raman imaging of amorphous-amorphous phase separation in small molecule co-amorphous systems. *European Journal of Pharmaceutics and Biopharmaceutics, 155*, 49–54.
Kong, W., Gao, Y., Liu, Q., Dong, L., Guo, L., Fan, H., Fan, Y., & Zhang, X. (2020). The effects of chemical crosslinking manners on the physical properties and biocompatibility of collagen type I/hyaluronic acid composite hydrogels. *International Journal of Biological Macromolecules, 160*, 1201–1211.
Kumar, S., Gokhale, R., & Burgess, D. J. (2014). Sugars as bulking agents to prevent nano-crystal aggregation during spray or freeze-drying. *International Journal of Pharmaceutics, 471*(1–2), 303–311.
Lim, A. S. L., Burdikova, Z., Sheehan, J. J., & Roos, Y. H. (2016). Carotenoid stability in high total solid spray dried emulsions with gum Arabic layered interface and trehalose–WPI composites as wall materials. *Innovative Food Science & Emerging Technologies, 34*, 310–319.
Lim, A. S. L., & Roos, Y. H. (2017). Carotenoids stability in spray dried high solids emulsions using layer-by-layer (LBL) interfacial structure and trehalose-high DE maltodextrin as glass former. *Journal of Functional Foods, 33*, 32–39.
Liu, X., Ji, Z., Peng, W., Chen, M., Yu, L., & Zhu, F. (2020b). Chemical mapping analysis of compatibility in gelatin and hydroxypropyl methylcellulose blend films. *Food Hydrocolloids, 104*, 105734.
Liu, Q., Mai, Y., Gu, X., Zhao, Y., Di, X., Ma, X., & Yang, J. (2020a). A wet-milling method for the preparation of cilnidipine nanosuspension with enhanced dissolution and oral bioavailability. *Journal of Drug Delivery Science and Technology, 55*, 101371.
Liu, X., Zhang, N., Yu, L., Zhou, S., Shanks, R., & Zheng, J. (2016). Imaging the phase of starch–gelatin blends by confocal Raman microscopy. *Food Hydrocolloids, 60*, 7–10.
Li, M., Yaragudi, N., Afolabi, A., Dave, R., & Bilgili, E. (2015). Sub-100nm drug particle suspensions prepared via wet milling with low bead contamination through novel process intensification. *Chemical Engineering Science, 130*, 207–220.
Lu, X., Xiao, J., & Huang, Q. (2018). Pickering emulsions stabilized by media-milled starch particles. *Food Research International, 105*, 140–149.
Lu, X., Zhang, H., Li, Y., & Huang, Q. (2017). Fabrication of milled cellulose particles-stabilized Pickering emulsions. *Food Hydrocolloids, 77*, 427–435.
Lv, Y., Zhang, L., Li, M., He, X., & Hao, L. (2019). Physicochemical properties and digestibility of potato starch treated by ball milling with tea polyphenols. *International Journal of Biological Macromolecules, 129*, 207–213.
Malamatari, M., Somavarapu, S., Bloxham, M., & Buckton, G. (2015). Nanoparticle agglomerates of indomethacin: The role of poloxamers and matrix former on their dissolution and aerosolisation efficiency. *International Journal of Pharmaceutics, 495*(1), 516–526.
Malamatari, M., Somavarapu, S., Taylor, K. M. G., & Buckton, G. (2016). Solidification of nanosuspensions for the production of solid oral dosage forms and inhalable dry powders. *Expert Opinion on Drug Delivery, 13*(3), 435–450.
Monteiro, A., Afolabi, A., & Bilgili, E. (2013). Continuous production of drug nanoparticle suspensions via wet stirred media milling: A fresh look at the rehbinder effect. *Drug Development and Industrial Pharmacy, 39*(2), 266–283.
Muhoza, B., Xia, S., Wang, X., & Zhang, X. (2020). The protection effect of trehalose on the multinuclear microcapsules based on gelatin and high methyl pectin coacervate during freeze-drying. *Food Hydrocolloids, 105*, 105807.
Penicaud, C., Peyron, S., Gontard, N., & Guillard, V. (2012). Oxygen quantification methods and application to the determination of oxygen diffusion and solubility coefficients in food. *Food Reviews International, 28*(2), 113–145.
Salminen, H., Ankenbrand, J., Zeeb, B., Badolato Bönisch, G., Schäfer, C., Kohlus, R., & Weiss, J. (2019). Influence of spray drying on the stability of food-grade solid lipid nanoparticles. *Food Research International, 119*, 741–750.
Semba, K., Kadota, K., Arima, H., Nakanishi, A., Tandia, M., Uchiyama, H., Sugiyama, K., & Tozuka, Y. (2019). Improved water dispersibility and photostability in folic acid nanoparticles with transglycosylated naringin using combined processes of wet-milling and freeze-drying. *Food Research International*, 108–116.
da Silva Carvalho, A. G., da Costa Machado, M. T., da Silva, V. M., Sartoratto, A., Rodrigues, R. A. F., & Hubinger, M. D. (2016). Physical properties and morphology of spray dried microparticles containing anthocyanins of jussara (Euterpe edulis Martius) extract. *Powder Technology, 294*, 421–428.
Spada, J. C., Norea, C. P. Z., Marczak, L. D. F., & Tessaro, I. C. (2012). Study on the stability of β-carotene microencapsulated with pinho (Araucaria angustifolia seeds) starch. *Carbohydrate Polymers, 89*(4), 1166–1173.
Wei, Y., Sun, C., Dai, L., Zhan, X., & Gao, Y. (2018). Structure, physicochemical stability and in vitro simulated gastrointestinal digestion properties of β-carotene loaded zein-propylene glycol alginate composite nanoparticles fabricated by emulsification-evaporation method. *Food Hydrocolloids, 81*, 149–158.
Wei, Y., Tong, Z., Dai, L., Ma, P., Zhang, M., Liu, J., Mao, L., Yuan, F., & Gao, Y. (2020). Novel colloidal particles and natural small molecular surfactants co-stabilized Pickering emulsions with hierarchical interfacial structure: Enhanced stability and controllable lipolysis. *Journal of Colloid and Interface Science, 563*, 291–307.
Wei, Y., Yu, Z., Lin, K., Sun, C., Dai, L., Yang, S., Mao, L., Yuan, F., & Gao, Y. (2019a). Fabrication and characterization of resveratrol loaded zein-propylene glycol alginate-rhamnolipid composite nanoparticles: Physicochemical stability, formation mechanism and in vitro digestion. *Food Hydrocolloids, 95*(OCT), 336–348.
Wei, Y., Zhang, L., Yu, Z., Lin, K., Yang, S., Dai, L., Liu, J., Mao, L., Yuan, F., & Gao, Y. (2019b). Enhanced stability, structural characterization and simulated gastrointestinal digestion of coenzyme Q10 loaded ternary nanoparticles. *Food Hydrocolloids, 94*, 333–344.
Wu, S., Fitzpatrick, J., Cronin, K., & Miao, S. (2019). The effect of pH on the wetting and dissolution of milk protein isolate powder. *Journal of Food Engineering, 240*, 114–119.
Wu, S., Pan, S., & Wang, H. (2014). Effect of trehalose on Lateolabrax japonicus myofibrillar protein during frozen storage. *Food Chemistry, 160*, 281–285.
Yamasaki, K., Kwok, P. C. L., Fukushige, K., Prud'homme, R. K., & Chan, H.-K. (2011). Enhanced dissolution of inhalable cyclosporine nano-matrix particles with mannitol as matrix former. *International Journal of Pharmaceutics, 420*(1), 34–42.
Zhan, X., Dai, L., Zhang, L., & Gao, Y. (2020). Entrapment of curcumin in whey protein isolate and zein composite nanoparticles using pH-driven method. *Food Hydrocolloids, 106*, 105839.
Zhang, Q., Yang, L., Hu, S., Liu, X., & Duan, X. (2019). Consequences of ball-milling treatment on the physicochemical, rheological and emulsifying properties of egg phosvitin. *Food Hydrocolloids, 95*, 418–425.
Zuo, B., Sun, Y., Li, H., Liu, X., & He, Z. (2013). Preparation and in vitro/in vivo evaluation of fenofibrate nanocrystals. *International Journal of Pharmaceutics, 455*(1–2), 267–275.